Carbohydrate Polymer Technologies and Applications 7 (2024) 100469

Contents lists available at ScienceDirect

Carbohydrate Polymer Technologies and Applications

journal homepage: www.sciencedirect.com/journal/carbohydrate-polymer-technologies-and-applications

Synthesis and comprehensive characterization with anticancer activity assessment of salicylaldehyde and 2-acetylphenol based chitosan thiosemicarbazones and their copper(II) complexes

Hari Sharan Adhikari [a], Aditya Garai [b], Chetana Khanal [c], Paras Nath Yadav [d,*]

[a] Department of Applied Sciences, Tribhuvan University, Institute of Engineering, Pashchimanchal Campus, Pokhara 33700, Nepal
[b] Department of Inorganic and Physical Chemistry, Indian Institute of Science, Bangalore 560012, India
[c] Central Department of Biotechnology, Tribhuvan University, Kathmandu 44600, Nepal
[d] Central Department of Chemistry, Tribhuvan University, Kathmandu 44600, Nepal

ARTICLE INFO

Keywords:
2-Acetyl phenol
Anticancer activity
Chitosan
Chitosan thiosemicarbazones
Copper(II) chitosan thiosemicarbazones
Functionalization
Salicylaldehyde

ABSTRACT

Functionalization of chitosan as salicylaldehyde and 2-acetylphenol-based chitosan thiosemicarbazone involving amino group at C2 position of pyranose ring was confirmed by comprehensive characterization by spectroscopic and analytical ways. Both the low molecular weight (*Mw*) chitosan oligosaccharide (CS) (*Mw* < 3000 *Da*, degree of deacetylation (*DDA*) = 87 %) and the crab shell chitosan (CCS) (*Mw* = 350 *kDa, DDA* = 67 %) functionalized thiosemicarbazones behaved as ONS tridentate ligand to form the square planar copper(II) complexes with a chloride ion as an additional ligand to satisfy the co-ordination sphere. All the derivatives were found thermally stable till the commencement of chitosan backbone disruption at 200 °*C*. The MTT assay profiles showed a conspicuous enhancement in the *in vitro* antitumorigenic and anticancer activity of native chitosan upon its functionalization as phenolic carbaldehyde chitosan thiosemicarbazones. Further, the assays more often revealed a further lowering of cell viability with chitosan oligosaccharide derivatives in comparison to high molecular weight chitosan derivatives, and a lower viability of the MCF-7 cancer cells than the tumorigenic MDCK cells. Both the low M_w chitosan with high *DDA* and high M_w chitosan with low *DDA*, the chitosan-functionalized salicylaldehyde based thiosemicarbazones, and their copper(II) chitosan thiosemicarbazone complexes were found to have minimal toxicity with IC_{50} >600 μgmL^{-1} against the mouse embryonic normal fibroblast NIH3T3 cells. These results were indicatives of more protonation and enhanced anticancer activity of chitosan oligosaccharide derivatives, and preferential cytotoxicity of chitosan biomaterials against the tumorigenic and cancer cells with more negatively charged cell surfaces.

Abbreviations

CS chitosan oligosaccharide
CCS crab shell chitosan
CSSTSC chitosan oligosaccharide salicylaldehyde thiosemicarbazone
Cu-CSSTSC copper(II) chitosan oligosaccharide salicylaldehyde thiosemicarbazone
CSAPTSC chitosan oligosaccharide 2-acetylphenol thiosemicarbazone
Cu-CSAPTSC copper(II) chitosan oligosaccharide 2-acetylphenol thiosemicarbazone
CCSSTSC crab shell chitosan salicylaldehyde thiosemicarbazone
Cu- CCSSTSC copper(II) crab shell chitosan salicylaldehyde thiosemicarbazone
CCSAPTSC Crab shell chitosan 2-acetylphenol thiosemicarbazone
Cu-CCSAPTSC copper(II) crab shell chitosan 2-acetylphenol thiosemicarbazone

1. Introduction

Chitosan is a multipurpose biomaterial obtained by more than 50 % deacetylation of chitin (Pillai et al, 2009) that is predominantly extracted from crustacean shells (Hafdani & Sadeghinia, 2011) and the bioactivity of chitosan shows a value-addition owing to its non-toxicity, biodegradability and biocompatibility (Nithya & Jothivenkatachalam, 2015; Cruz-Romero et al., 2013; Anitha et al., 2014). Chitosan oligosaccharide with a lower molecular weight (M_w) and a greater degree of

* Corresponding author.
E-mail address: paras.yadav@tu.edu.np (P.N. Yadav).

https://doi.org/10.1016/j.carpta.2024.100469

Available online 28 February 2024

deacetylation (*DDA*) has been reported to show better permeation through the cancer cell surfaces (Zhang et al., 2010) and a subsequent attack to cancer cells by the process of endocytosis (Huang et al., 2004; Wimardhani et al., 2014). But a separate study has shown that there is no significant effect of M_w of chitosan in the range of 100–800 *kDa* on its *in vitro* anticancer activity against the human breast cancer (MCF-7) cell lines (Abedian et al., 2019). These results are indicatives of almost no effect of change in M_w of polymeric chitosan in a certain range above a certain weight of chitosan (Abedian et al., 2019). The higher anticancer activity of low molecular weight chitosan is associated with more protonation of its amino group at C2 position of the ring and selective permeation through more negatively charged cancer cell surfaces (Zhang et al., 2010). The current study involves assessment of anticancer activity of chitosan-functionalized thiosemicarbazones and their copper (II) complexes with chitosan weight of 3 *kDa* and 350 *kDa*. So, the derivatives with low and high molecular weight chitosan constituents could bring about the differences in anticancer activity of chitosan derivatives.

Functionalization of chitosan that involves amino and acetamido moieties of glucosamine monomers has been found to bring about an enhancement in water-solubility, chelation with metal ions, and electrostatic interaction with cell surfaces (Adhikari & Yadav, 2018). Grafting of several carboxaldehyde thiosemicarbazone moieties in chitosan (Adhikari et al., 2021; Adhikari et al., 2022; Adhikari et al., 2022) was previously found to bring an enhancement in anticancer activity of chitosan and a further increase in anticancer activity was observable upon the coordination of these chitosan functionalized thiosemicarbazones with copper(II) ion. Further, chitosan is a cationic polysaccharide that undergoes permeation through the negatively charged membranes of cancer cells and shows anticancer activity by cellular apoptotic, antiangiogenic, and immunoenhancement pathways (Adhikari & Yadav, 2018). Chitosan as a free ligand also shows coordination behavior with copper(II) ion and the chitosan-copper complexes have been investigated as advanced anticancer materials (Usman et al., 2012; Wu et al., 2009; Tokarek et al., 2013). Copper has been found in higher concentration in cancer cells than in healthy cells (Yoshida et al., 1993; Geraki et al., 2002) showing the phenomenal involvement of copper in the processes of tumor growth, metastasis and angiogenesis (Xie & Kang, 2009). Segregation of copper ions from the tumor cells by employing them in chelation and formation of antitumor copper complexes is crucial towards the anticancer drug development strategy (Santini et al., 2014). Thiosemicarbazones (TSCs) are the potent anticancer ligands which can selectively permeate through the tumor cell surfaces (Singh et al., 2020) and maintain the homeostasis of copper level in cells *via* the chelation with copper(II) ions (Santini et al., 2014; Denoyer et al., 2015). Anticancer activity of TSCs has also been associated with the interference to deoxyribonucleic acid (DNA) synthesis *via* the ribonucleotide reductase (RR) inhibition (Gojo et al., 2007; Finch et al., 2000), the cell cycle arrest (Rao et al., 2009) and an increment in the expression of reactive oxygen species (ROS) (Malarz et al., 2018). Salicylaldehyde-based TSCs that essentially behave as tridentate ligands (Zhang et al., 2016; Carcelli et al., 2020) were found to have a conspicuous anticancer activity associated with the inhibition of copper-binding protein disulfide isomerase (PDI) (Carcelli et al., 2020), an enzyme in endoplasmic reticulum (ER) that supports protein folding and proliferation of cancer cells (Yang et al., 2022).

Salicylaldhyde thiosemicarbazone has been found to cause higher *in vitro* activity against MCF-7 cancer cell line, but a low cytotoxicity against the normal MCF-10 cells (Sibuh et al., 2020). The concentration dependent growth inhibitory activity of salicylaldehyde-based TSCs against the cancer cells has been found to be affected by the substituents in benzene ring, structural variation, type of cancer cells, and dose (Zhang et al., 2016; Carcelli et al., 2020; Yang et al., 2022; Zhang et al., 2010). The TSCs with different carboxaldehyde moieties and the substituents show variations in their anticancer activity associated with different mechanisms of action, and there is structure-activity relation that governs the specificity in anticancer pathways. For instance, the anticancer activity of chitosan functionalized isatin-based TSCs shows synergistic contribution from isatin scaffold towards inhibition of tubulin and microtubules formation (Jordan & Wilson, 2004; Vindya et al., 2015), inhibition of receptor tyrosine kinases (RTKs) and cyclin-dependent kinases (CDKs) (Sun et al., 2003; Polychronopoulos et al., 2004) and the specificity of salicylaldehyde-based carbonyl moiety in the TSCs lies on inhibition of PDI (Carcelli et al., 2020) and anti-proliferation of cancer cells (Yang et al., 2022). Anticancer activity of copper(II)- thiosemicarbazone complexes is associated with their behavior to cause intercalation between DNA base pairs, DNA cleaving and apoptosis to bring about the inhibition of angiogenesis (Singh et al., 2020; Wang et al., 2010). Copper(II)-thiosemicarbazone complexes bring about the inhibition of topoisomerase II and exhibit higher anticancer activity than the free thiosemicarbazone ligands (Singh et al., 2020). Anticancer and cytotoxic function of metal-thiosemicarbazone complexes is also dependent upon the type of metals, and its chelation to free ligand. For instance, palladium(II) 1-naphthaldehyde based thiosemicarbazones have been found to show higher anticancer activity than the free ligands. The anticancer activity of these complexes may have been closely associated with intercalation between the base pairs and cleaving of DNA (Hernández et al., 2016) showing the resemblance with the activity of copper(II) thiosemicarbazones. The cytotoxicity of copper(II) complexes of 1-[amino(thioxo)methyl]−5-hydroxy-3-methyl-1H-pyrazole has been found far more than the corresponding nickel(II) and cobalt(II) complexes (Sobiesiak et al., 2016).

The tumorigenic phenotype of Madin-Darby Canine Kidney (MDCK) cell line obtainable from the normal kidney cells (Omeir et al., 2011) and MCF-7, the human breast cancer cell line with comparatively more negatively charged cell surfaces (Faris et al., 2021; Comsa et al., 2015; Zhou et al., 2015) could show less viability with the anticancer chitosan derivatives. Based on these grounds, the current work comprised the study of *in vitro* anticancer activity of salicylaldehyde and 2-acetylphenol based chitosan functionalized thiosemicarbazones and their copper (II) complexes against the tumorigenic Madin-Darby Canine Kidney (MDCK) and human breast cancer (MCF-7) cell lines. Both the chitosan oligosaccharide (CS) and high molecular weight crab shell chitosan (CCS) were grafted into phenolic carbaldehyde thiosemicarbazones to get the derivatives with the anticancer effects of the constituent moieties synergized. Then, the respective copper(II) chitosan thiosemicarbazones were synthesized as the complexes with further enhanced anticancer activity. Overall, the study was oriented with the motivation towards the tailoring of chitosan-functionalized compounds in a quest to get structurally elucidated derivatives of conspicuous anticancer activity, and these materials could stand as strategically favorable anticancer alternatives with minimal side effects. The reports evidently in support of this research orientation could be met up, for instance, with higher activity of both low and high molecular weight chitosan (300–800 *kDa* range) against MCF-7 cancer cells and minimal activity of these chitosan materials against the normal human fibroblast cells (Abedian et al., 2019). The objectives of the study were to synthesize the novel chitosan derivatives *viz.* chitosan functionalized salicylaldehyde based thiosemicarbazones and prepare their copper(II) complexes in an expectation to get the derivatives of conspicuous anticancer activity. The study aimed at enhancement of anticancer activity of native chitosan upon its tailoring as chitosan functionalized thiosemicarbazones, and further enhancement of the activity upon coordination with copper (II) ion. The suitability of native chitosan with low and high molecular weights and phenolic carboxaldehyde was rationalized on the basis of their anticancer effects and the expected synergistic effects towards the overall activity of the derivatives. The current study leaves the area of further investigation towards the mechanisms of action of anticancer activity of these chitosan-functionalized materials.

2. Materials and methods

2.1. Materials

Chitosan oligosaccharide, ($C_{12}H_{24}N_2O_9$) n (87 % *DDA, Mw* < 3000 *Da*) from Sisco Research Laboratories Pvt. Ltd., Maharashtra, India; crab shells from municipal wet market of Kathmandu, Nepal; salicylaldehyde, 2-acetyl phenol (Sigma-Aldrich), acetic acid glacial (Merck 100%), sodium acetate (Merck), sodium hydroxide (Merck, 99 %), hydrochloric acid (Merck 99%), copper(II) chloride (Merck), ethanol (Sigma-Aldrich, 99.80%), carbon disulphide (s d fine-chem limited), hydrazine monohydrate, sodium chloroacetate and acetone (Thermo Fisher Scientific); ammonium hydroxide, methanol, and other analytical grade reagents used with no further purification. The Madin-Darby Canine Kidney (MDCK) cell line with the expression of immortalized tumorigenic phenotype and the human breast cancer (MCF-7) cell line and the mouse embryonic normal fibroblast (NIH3T3) cells were purchased from Shikhar Biotech, Lalitpur, Nepal. The requirements for the complete RPMI media (a mixture of 1.2 % solution of Penicillin and Streptomycin antibiotics, 10 % fetal bovine serum (FBS), 25 mM 4-(2-hydroxyethyl)−1-piperazineethanesulfonic acid (HEPES) and an incomplete RPMI media with glutamine), phosphate buffer solution (PBS), dimethyl sulfoxide (DMSO), the tetrazolium dye 3-(4,5-dimethylthiazol-2-yl)−2,5-diphenyltetrazolium bromide (MTT) were purchased from Rani Sati Trading, Kathmandu, Nepal.

2.2. Measurements

The FT-IR spectra: taken in powder state with BRUKER 1 003 3610 FT-IR spectrophotometer ATR-GeXPm experimentation in the regions 4000–400 cm^{-1}. The solid state ^{13}C NMR spectra: taken in BRUKER AC-800 Delta 2 NMR spectrometer with cross polarization, scans 276 and contact time of 3.5 *mins*, at a field strength 9.389766[*T*] (400[*MHz*]). Powder X Ray Diffraction (PXRD) measurements: taken in a D8 advance BRUKER diffractometer, scanning scope of 2θ at 0–60°, exposed for 400 *S*, Cu target (*λ*= 0.1541 *nm*) at 40 *KV*. Elemental analyses: performed with a Thermo Finnigan FLASH EA 112CHNS microanalyzer, carrier gas He (140 *mL*/min), CHNS/ NCS column PQS SS 2 M 6 × 5 *mm* in an oven at 75 °*C*. Thermal data: taken with a temperature rise of 10 °*C* per minute using DTA/TG Al crucible. Magnetic susceptibility of the complexes: effective magnetic moment (μ_{eff}) measured by Sherwood Scientific, Cambridge, UK; X1 range setting magnetic susceptibility balance with the powdered sample filled up to 1.5 *cm* (L) of a weighing tube, the weight of the empty weighing tube = 0.8233 *g*. EPR spectra: taken with Bruker biospin corp (EMX series) Model: A 200–9.5/12B/S spectrometer at a field set 3000 *Gs*, X band frequency of 9.8577–9.8630 *GHz* and a scan range of 2000 *Gs*.

The thermal and EPR spectroscopic data of complexes were taken at the Department of Chemistry, Korea Center for Artificial Photosynthesis (KCAP), Center for Nanomaterial, Sogang University, Shinsu-dong, Mapogo, South Korea. The FT-IR, ^{13}C NMR spectra, elemental analyses, PXRD, magnetic susceptibility and thermal data (of the ligands) were taken at Indian Institute of science (IISc), Bangalore, India. The cells culturing and colorimetric MTT assays were performed at Central Department of Biotechnology, Tribhuvan University, Kirtipur, Kathmandu, Nepal.

2.3. Experimental

2.3.1. Syntheses of phenolic carbaldehyde chitosan thiosemicarbazones

Chitosan thiosemicarbazones *viz* salicylaldehyde oligo-chitosan thiosemicarbazone (CSSTSC) and salicylaldehyde crab shell chitosan thiosemicarbazone (CCSSTSC), 2-acetylphenol oligo-chitosan thiosemicarbazone (CSAPTSC) and 2-acetylphenol crab shell chitosan thiosemicarbazone (CCSAPTSC) were synthesized *via* the formation of chitosan thiosemicarbazide. The synthesis of chitosan thiosemicarbazide was carried out with minor modifications through the formation of ammonium dithiocarbamate chitosan and sodium carbethoxydithiocarbamate chitosan (Muzzarelli et al., 1982). For this, a mixture of 2 *g* of chitosan and 3 *mL* of ethanolic ammonia solution was stirred at room temperature for one and half hour and 2 *mL* of carbon disulphide were added in little instalments and stirred at room temperature for three hours to get ammonium dithiocarbamate chitosan. Then, sodium chloroacetate (2.85 *g*) was added, the mixture was stirred at room temperature for two hours, hydrazine monohydrate (2 *mL*) was added drop wise, and the mixture was further stirred at room temperature for four hours to get sodium carbethoxydithiocarbamate chitosan. It was washed with ethanol and filtered up to dryness to get a brown residue of chitosan thiosemicarbazide recovered (Muzzarelli et al., 1982). Next, the one pot synthetic reaction was accomplished by the reflux condensation of an equimolar mixture of chitosan thiosemicarbazide and carboxaldehyde (salicylaldehyde or 2-acetyl phenol) at 65 °*C* for 12 *h* in the presence of acetic acid as a catalyst. The resultant mixture was cooled down and filtered and washed with methanol, and again filtered up to dryness to get chitosan functionalized as chitosan thiosemicarbazone.

The functionalization of chitosan as chitosan thiosemicarbazone (scheme 1) involves the partial incorporation of thiosemicarbazone moiety into chitosan, and a Schiff's reaction of phenolic carbaldehyde with amino group in C-2 position of the ring chitosan (Adhikari et al., 2021; Adhikari et al., 2022; Adhikari et al., 2022; Zhong et al., 2010).

The partial incorporation *via* the Schiff's addition of phenolic carbaldehyde moiety into chitosan at C2 position of the pyranose ring was shown by the degree of substitution (*DS*) values. For chitosan oligosaccharide (unit weight 166, *DDA* 87 %) functionalized thiosemicarbazone (TSC), $DS = \frac{(166\ X\%\ (S)}{(3200-Mtsc\ X\%(S)}$ and for crab shell chitosan (unit weight 171, *DDA* 67 %), $DS = \frac{(171\ X\%\ (S)}{(3200-Mtsc\ X\%(S)}$ where%(S) is sulphur percentage (found), Mtsc is thiosemicarbazone unit weight (Adhikari et al., 2022; Pires et al., 2013).

2.3.1.1. Chitosan oligosaccharide salicylaldehyde thiosemicarbazone (CSSTSC). Yield: 38 %; color: Yellowish; *m. p.* > 300 °*C*: decomposed into brown residual mass; calc. for $C_{14}H_{17}N_3O_5S$ (unit formula wt. 339, chitosan unit 160.16) C, 49.55; H, 5.01; N, 12.38 and S, 9.43 %; found (for 87 % *DDA* of chitosan) C, 55.10; H, 5.201; N, 10.00 and S, 3.150%; *DS*: 19.83 %; IR (cm^{-1}, s: strong, m: medium, w: weak): *ν*(O—H) and *ν*(N—H) stretches merged with a broad translocation 3225 s, *ν*(C=N) 1625s, *ν*(N-H) bend 1567 m, *ν*(C-H) bend1487s, *ν*(C=S) 1055s, 1374s and *ν*(phenolic C—O) 1268s; *δ* (^{13}C NMR, 400 *MHz, ppm*) = 24.62 (CH_3), 62.14 (C6), 75.81 (C3, C5), 84.44 (C4), 104.36 (C1), 130–160 (phenyl ring C—H), 173.23 (HC=N-) and 178.96 (C=S & C=O superimposition).

2.3.1.2. Crab shell chitosan salicylaldehyde thiosemicarbazone (CCSSTSC). Yield: 32 %; color: yellowish white; *m. p.* > 300 °*C*: decomposed into brownish black residual mass; calc. for $C_{14}H_{17}N_3O_5S$ (unit formula wt. 339, chitosan unit 160.16); C, 49.55; H, 5.01; N, 12.38 and S, 9.43 %; found (for 67 % *DDA* of chitosan) C, 54.216; H, 5.135; N, 10.823 and S, 3.021 %; *DS*: 19.42 %; IR (cm^{-1}, s: strong, m: medium, w: weak): *ν*(O—H) and *ν*(N—H) stretches merged with a broad translocation 3240 m, *ν*(C=N) 1618s, *ν*(N-H) bend 1556s, *ν*(C-H) bend 1486s, *ν*(C=S) 894 s, 1380s and *ν*(phenolic C-O) 1275s; *δ* (^{13}C NMR, 400 *MHz, ppm*) = 22.99 (CH_3), 64.95 (C6), 73.50 (C3, C5), 83.51 (C4), 104.27 (C1), 119–164 (phenyl ring C-H), 173.93 (HC=N-) and 200.94 (C=S & C=O superimposition).

2.3.1.3. Chitosan oligosaccharide 2-acetylphenol thiosemicarbazone (CSAPTSC). Yield: 46 %; color: yellow; *m. p.* > 300 °*C*: decomposed into brown residual mass; calc. for $C_{15}H_{19}N_3O_5S$ (unit formula wt. 353, chitosan unit 160.16) C, 51.28; H, 5.41; N, 11.96 and S, 9.11 %; found (for 87 % *DDA* of chitosan) C, 53.10; H, 5.87; N, 8.98 and S, 4.47 %; *DS*: 31.68 %; IR (cm^{-1}, s: strong, m: medium, w: weak): *ν*(O—H) and

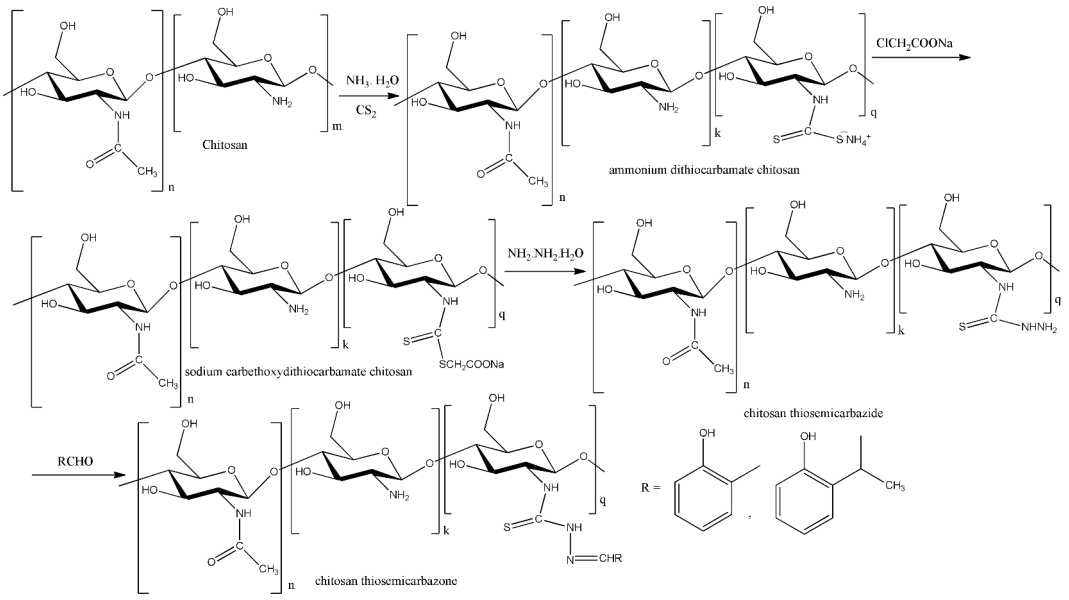

Scheme 1. : Synthetic route of functionalization of chitosan as chitosan thiosemicarbazones.

ν(N—H) stretches merged with a broad translocation 3292 m, ν(C=N) 1612 m, ν(N-H) bend 1558s, ν(C-H) bend 1489s, ν(C=S) 1078 w, 1361 m and ν(phenolic C-O) 1251s; δ (^{13}C NMR, 400 *MHz, ppm*) = 23.50 (CH_3), 62.08 (C6), 75.15 (C3, C5), 83.33 (C4), 102.01 (C1), 119–162 (phenyl ring C-H), 168.43 (HC=N-) and 176.25 (C=S & C=O superimposition).

2.3.1.4. Crab shell chitosan 2-acetylphenol thiosemicarbazone (CCSAPTSC). Yield: 39 %; color: yellowish white; *m. p.* > 300 °*C*: decomposed into brownish black residual mass; calc. for C_{15} H_{19} N_3O_5S (unit formula wt. 353, chitosan unit 160.16) C, 51.28; H, 5.41; N, 11.96 and S, 9.11 %; found (for 67% *DDA* of chitosan) C, 52.01; H, 5.74; N, 8.86 and S, 4.38 %; *DS*: 31.74 %; IR (cm^{-1}, s: strong, m: medium, w: weak): ν(O—H) and ν(N—H) stretches merged with a broad translocation 3300 m, ν(C=N) 1611s, ν(N-H) bend 1555s, ν(C-H) bend 1439s, ν(C=S) 841 s, 1360s and ν(phenolic C-O) 1241s; δ (^{13}C NMR, 400 *MHz, ppm*) = 22.81 (CH_3), 61.04 (C6), 73.39 (C3, C5), 83.28 (C4), 104.07 (C1), 119–162 (phenolic ring C-H), 167.40 (HC=N-) and 172.92 (C=S & C=O superimposition).

2.3.2. Preparation of copper(II) chitosan thiosemicarbazones

A mixture of 1 *mmol* each of chitosan thiosemicarbazone and copper (II) chloride maintained at pH 6 by addition of 1 % acetic acid was stirred for three hours at 65 °*C*. The mixture was filtered and the complex obtained as a residue was dried overnight at 40 °*C*. This process of preparation of copper(II) chitosan thiosemicarbazones (Adhikari et al., 2021; Adhikari et al., 2022; Adhikari et al., 2022) employed minor modifications in the reported method of preparation of copper (II)-chitosan complexes (Zheng et al., 2006). Estimation of chlorine percentages in the complexes was made by the method of potentiometric titrations (Tiwari et al., 2016).

2.3.2.1. Copper(II) chitosan oligosaccharide salicylaldehyde thiosemicarbazone (Cu-CSSTSC). Yield: 70 %; color: greenish yellow; *m. p.* > 300 °*C*: decomposed into greyish residue; calc. for C_{14} H_{17} N_3O_5SCuCl (unit formula wt. 438, chitosan unit 160.16) C, 38.35; H, 3.88; N, 9.58; S, 7.30 and estimated Cl, 8.10 %; found (for 87 % *DDA* of chitosan) C, 44.04; H, 4.019; N, 7.74; S, 2.214 % and estimated Cl, 10.50 %; IR (cm^{-1}, s: strong, m: medium, w: weak): ν(O—H) and ν(N—H) stretches merged with a broad translocation 3021 m, ν(C=N) 1616s, ν(N-H) bend 1536s, ν(C=S) 1030 m, 1324 m and ν(phenolic C—O) 1260 m; Effective magnetic moment (μ_{eff}) (*B. M.*): 1.80; EPR (*g* value): 2.07 (ν = 9.8623 *GHz*, B_o =3400 *Gs* = 340 *mT*).

2.3.2.2. Copper(II) crab shell chitosan salicylaldehyde thiosemicarbazone (Cu-CCSSTSC). Yield: 67 %; color: greenish yellow; *m. p.* > 300 °*C*: decomposed into greyish black residue; calc. for C_{14} H_{17} N_3O_5SCuCl (unit formula wt. 438, chitosan unit 160.16) C, 38.35; H, 3.88; N, 9.58; S, 7.30 and estimated Cl, 8.10 %; found (for 67 % *DDA* of chitosan) C, 44.50; H, 5.201; N, 10.325; S, 2.012 % and estimated Cl, 10.50 %; IR (cm^{-1}, s: strong, m: medium, w: weak): ν(O—H) and ν(N—H) stretches merged with a broad translocation 3019 m, ν(C=N) 1611s, ν(N-H) bend 1533s, ν(C=S) 860 w, 1320 and ν(phenolic C—O) 1196s; Effective magnetic moment (μeff) (*B. M.*): 1.85; EPR (*g* value): 2.10 (ν =9.8630 *GHz*, B_o = 3350 *Gs* = 335 *mT*).

2.3.2.3. Copper(II) chitosan oligosaccharide 2-acetylphenol thiosemicarbazone (Cu-CSAPTSC). Yield: 72 %; color: yellowish green; *m. p.* > 300 °*C*: decomposed into brownish residue; calc. for C_{15} H_{19} N_3O_5SCuCl (unit formula wt. 452, chitosan unit 160.16) C, 39.82; H, 4.20; N, 9.29; S, 7.07 and estimated Cl, 7.85 %; found (for 87 % *DDA* of chitosan) C, 44.35; H, 5.104; N, 8.84; S, 2.351 % and estimated Cl, 10.05 %; IR (cm^{-1}, s: strong, m: medium, w: weak): ν(O—H) and ν(N—H) stretches merged with a broad translocation 3290 s, ν(C=N) 1602s, ν(N—H) bend 1563s, ν(C=S) 1037 m, 1353 m and ν(phenolic C—O) 1232s; Effective magnetic moment (μ_{eff}) (*B. M.*): 1.82; EPR (*g* value): 2.09 (ν = 9.8623 *GHz*, B_o = 3359 *Gs* = 335.9 *mT*).

2.3.2.4. Copper(II) crab shell chitosan 2-acetylphenol thiosemicarbazone (Cu-CCSAPTSC). Yield: 66 %; color: yellowish green; *m. p.* > 300 °*C*: decomposed into greyish residue; calc. for $C_{15}H_{19}N_3O_5SCuCl$ (unit formula wt. 452, chitosan unit 160.16) C, 39.82; H, 4.20; N, 9.29; S, 7.07 and estimated Cl, 7.85 %; found (for 67 % *DDA* of chitosan) C, 44.20; H, 5.09; N, 8.902; S, 2.29 % and estimated Cl, 10.05 %; IR (cm^{-1}, s: strong, m: medium, w: weak): ν(O—H) and ν(N—H) stretches merged with a broad translocation 3276 s, ν(C=N) 1604s, ν(N—H) bend 1557s, ν(C = S) 829 m, 1354 m and ν(phenolic C—O) 1235s; Effective magnetic moment (μ_{eff}) (*B. M.*): 1.84; EPR (*g* value): 2.09 (ν = 9.8628 *GHz*, B_o = 3356 *Gs* = 335.6 *mT*).

2.3.3. Colorimetric MTT assays

The complete RPMI media for culturing of the cells was prepared as a mixture of 1.2 % solution of Penicillin and Streptomycin antibiotics, 10

% fetal bovine serum (FBS), 25 mM 4-(2-hydroxyethyl)−1-piperazineethanesulfonic acid (HEPES) and an incomplete RPMI media with glutamine. The cell line was cultured in the complete media with 5 % carbon dioxide for 24 *h*. The cellular debris from the cultured cells were washed away with phosphate buffer solution (PBS) and in a fresh medium, the cells were counted and distributed in the 96 well plate with $\sim 10^5$ cells in each well. The test solutions in dimethyl sulfoxide (DMSO) (50–600 $\mu g mL^{-1}$) with the cultured cells were incubated for 48 *h* and the tetrazolium dye 3-(4,5-dimethylthiazol-2-yl)−2,5-diphenyltetrazolium bromide (MTT) solution in PBS (5 *mg/mL*) was added in each well. Next, the solutions comprising the sample treated cells and MTT were incubated at 37 °*C* in CO_2 for 4 *h* until the purple crystals of formazan in the intracellular spaces was visible under microscope. The remaining yellow tetrazole MTT was removed and the formazan crystals were dissolved in DMSO. The solutions of formazan in DMSO were then triturated and incubated in CO_2 for 30 min at 37 °*C* until the lysing of the cells and dissolution of formazan to give purple solutions. The intensity of the purple-colored solutions was quantified using the ELISA plate reader at 551 *nm* absorbance. The absorbance due to sample treated cells (sample abs.) and absorbance due to untreated cells (control abs.) as the positive control were noted and the percentage cell viability was determined by:% *viable cells* $= \frac{(Sample\ abs. - Blank\ abs.)}{(Control\ abs - Blank\ abs.)} X\ 100$. The half inhibitory concentration (IC_{50}) was determined as the concentration at half the maximum absorbance (Kumar et al., 2018).

3. Results and discussion

3.1. Characterization

3.1.1. Fourier transform- infrared (FT-IR) spectroscopy

The FT-IR spectra of salicylaldehyde and 2-acetylphenol chitosan thiosemicarbazones (Figs. S1, S3, S5 & S7 in supporting information) showed a broad translocation due to ν(O—H) and ν(N—H) merged at a range of 3100–3300 cm^{-1} (Qin et al., 2012; Zhong et al., 2011). Disappearance of ν(C=O) of amide I at 1645 cm^{-1} (Qin et al., 2012) and the appearance of new band in the range of 1611–1625 cm^{-1} in the ligands were indicatives of the involvement of C=O group in imine (-C=N-) bond formation (Qin et al., 2012). Partial involvement of NH_2 group in the formation of thiosemicarbazones was shown by $\nu(NH_2)$ at 1555–1567 cm^{-1} (Yadav & Shivakumar, 2012) and ν(C=S) in two separate ranges of 841–1078 cm^{-1} (Tiwari et al., 2016; Yamaguchi et al., 1958) and 1360–1380 cm^{-1} (Aneesrahman et al., 2019; Joseph et al., 2006). The existence of thiosemicarbazones in thione form was shown by the absence of ν(C-SH) band at 2500–2600 cm^{-1} (Bharti et al., 2003). The absorption bands at 660–1100 cm^{-1} were attributed to ν(phenyl) from carboxaldehyde (Qin et al., 2012) and the bands at 1438–1489 cm^{-1} were corresponding to characteristic stretch ν(CH) of methylene to methyl groups (Kumari et al., 2016; Kumirska et al., 2010) in the ligands. There was weakening of residual peak due to acetamido moiety of chitin at 1550–1558 cm^{-1} (Zhong et al., 2010).

In the FT-IR spectra of copper(II) complexes (Figs. S2, S4, S6 & S8 in supporting information), the absorption peaks due to ν(OH) and ν(NH) were shifted to lower wave lengths at 3000–3200 cm^{-1} (Qin et al., 2012; Zhong et al., 2011) indicating the involvement of oxygen in coordination. The absence, or else the highly diminished intramolecular hydrogen band ν(OH) at 3284 cm^{-1} in the complexes indicated the deprotonation of phenolic-OH group (Sarker et al., 2019). The ν(phenolic C—O) vibration in the ligands at 1241–1275 cm^{-1} (Ismail et al., 2014) was lowered to 1196–1260 cm^{-1} indicating the involvement of OH group in complex formation. Lowering of ν(C=N) from 1611 to 1625 cm^{-1} (Qin et al., 2012) in ligand to 1602–1616 cm^{-1} in complexes showed the involvement of C=N group in complex formation. The negative shifting of peaks due to ν(C=S) to 829–1037 cm^{-1} (Wiles et al., 1967) and 1320–1354 cm^{-1} (Joseph et al., 2006) in the corresponding complexes showed the coordination of sulphur with metal ion. The overall impression of IR data indicated the partial grafting of thiosemicarbazone group into chitosan, and bonding of metal ion with thiosemicarbazones through phenolic oxygen, imino nitrogen and thione sulphur. This phenomenon accorded with the completion of the coordination sphere of copper(II) ion by mono-deprotonated O,N,S tridentate salicylaldehyde thiosemicarbazone ligand and a chloride ion (Carcelli et al., 2020).

3.1.2. Solid state ^{13}C nuclear magnetic resonance (^{13}C NMR) spectroscopy

The solid state ^{13}C NMR spectra of chitosan thiosemicarbazones (Figs. S9-S12 in supporting information) were compared with the solid state ^{13}C NMR spectra of unfunctionalized chitosan comprising the reported signals at 23–25 *ppm* (methyl group in acetamido moiety), 57- 60 *ppm* (C2), 60- 63 *ppm* (C6), 75–78 *ppm* (C3, C5), 83–84 *ppm* (C4), 104–106 *ppm* (C1 of the ring), and 174–178 *ppm* (due to C=O indicative of an incomplete deacetylation) (Qin et al., 2012; Adhikari et al., 2021; de Britto & Assis, 2007), and the comparison of these spectra was essentially used to elucidate the modification in chitosan ring structure (De Angelis et al., 1998). The weakening of C2 of chitosan signal at δ=57 *ppm* or the appearance of C2 signals in its neighborhood and the simultaneous appearance of -N=CH signal at δ= 167.40 −173.934 *ppm* showed the amino group substitution at C2 *viz*. the partial incorporation of C2 towards the imine bond formation (Qin et al., 2012; Wang et al., 2016). The partial deacetylation was shown by C=O signals (Wang et al., 2016) at a range of δ= 172.92–200.941 ppm. The characteristic peaks corresponding to ring chitosan in these chitosan thiosemicarbazones were evident from CH_3 (22.81–24.62 *ppm*), C6(61.04–64.956 *ppm*), C3, C5(73.39–79.731 *ppm*), C4(83.28–84.44 *ppm*), and C1(102.01–104.358 *ppm*) (Qin et al., 2012; Wang et al., 2016); and the phenyl carbon signals at δ= 130–160 *ppm* in CSSTSC, 119–164 *ppm* in CCSSTSC, 119–162 *ppm* in CSAPTSC, and 119–162 *ppm* in CCSAPTSC (Qin et al., 2012). The broadening of peak at a range of 172.92–200.941 *ppm* was indicative of the superimposition of C=S and C=O signals (Qin et al., 2012). These results were in agreement with the formation of thiosemicarbazone *via* the partial introduction of thiosemicarbazone moiety to C2 position of the ring chitosan.

3.1.3. Powder X ray diffraction (PXRD) studies

The X Ray diffractograms of chitosan thiosemicarbazones (Fig. S13-S16 in supporting information), with the distinct reflection peaks at 2θ = 15.39–25.30° in CSSTSC, 2θ = 11.39–26.91° in CCSSTSC, 2θ = 8.40°−29. 98° in CSAPTSC, and 2θ = 9.2–29.40° in CCSAPTSC showed the formation of new crystallinity phases due to formation of thiosemicarbazones (Hanumantharao et al., 2012; Santhakumari et al., 2010). The incorporation of thiosemicarbazone group in chitosan without destruction of the original crystallinity of chitosan was justifiable from shifting of peaks to neighborhood of chitosan peaks at 10° and 20° (Qin et al., 2012; Ramya et al., 2012) and the change in crystallinity pattern with the appearance of several other peaks (Qin et al., 2012). The formation of imine group and cleavage of intra-molecular hydrogen bond of chitosan have been reported to bring about the appearance of the new crystalline peaks (Jiao et al., 2011). The X ray diffractograms of copper(II) chitosan thiosemicarbazone complexes (Figs. S17-S20 in supporting information) showed the shifting of crystallinity pattern from that of the respective ligands. New peaks at 2θ = 12.57°,19.98° and 25.07°in Cu-CSSTSC, 2θ = 13.92°,18.89° and 25.36° in Cu-CCSSTSC, 2θ = 14.26°,19.98° and 24.14° in Cu-CSAPTSC, 2θ = 12.96°,19.82°,29.00° and 40.22° in Cu-CCSAPTSC were attributed to the formation of new crystalline phases, chelation of metal ion with different groups of thiosemicarbazone ligand and the destruction of existing crystallinity (Qin et al., 2012; Antony et al., 2012; Dehaghi et al., 2014; Mekahlia & Bouzid, 2009; Wang et al., 2005). The destruction of hydrogen bonds in chitosan owing to chelation of metal ions with amino or hydroxy group has been reported to bring about the formation of new crystallinity phases and the subsequent weakening or shifting of crystallinity peaks of chitosan at 10.4° and 19.8° (Wang et al., 2005). The crystalline sizes

corresponding to highest intensity peaks in X ray diffraction curves from *Debye-Scherrer formula*, (Mekahlia & Bouzid, 2009; Kucukgulmez et al., 2011) and the degree of crystallinity (Kumirska et al., 2010; Lomadze & Schneider, 2005; Zhang et al., 2005) as the crystallinity index were determined. The crystalline sizes of salicylaldehyde-based chitosan thiosemicarbazones (15.53–16.57 *nm*) were found less than 2-acetyl phenol-based chitosan thiosemicarbazones (22.28–24.76 *nm*). The crystallinity index was 72.84 % in CSSTSC, 71.97 % in CCSSTSC, 42.96 % in CSAPTSC, and 42.26 % in CCSAPTSC. It showed more crystallinity index with the decrease in crystalline size of the ligands. The crystalline sizes of copper(II) chitosan thiosemicarbazone complexes were found to be 9.02 *nm* in Cu-CSSTSC, 10.20 *nm* in Cu-CCSSTSC, 4.88 *nm* in Cu-CSAPTSC, and 6.39 *nm* in Cu-CCSAPTSC. The degree of crystallinity ranged from 45.12 to 47.77 % in salicylaldehyde complexes, and 49.47–51.15 % in 2-acetylphenol complexes. These results showed the decrease in crystalline size upon the complex formation, but the crystallinity index was not found only dependent on crystalline size in complexes. The powder X ray diffraction data of chitosan thiosemicarbazones and their copper(II) complexes: salicylaldehyde and 2-acetylphenol analogues are presented in Table 1. Appearance of new crystalline peaks in X ray diffractograms of the complexes showed the shifting of crystallinity pattern from chitosan thiosemicarbazone. Chelation of metal ion with different groups of thiosemicarbazone and the modification in existing crystallinity was shown by overall differences in crystallinity (Jiao et al., 2011). Further shifting of characteristic peaks derived from chitosan showed the new molecular arrangement in crystalline complexes.

3.1.4. Elemental microanalysis

The calculated percentages of elements in the ligands CSSTSC and CCSSTSC with the monomer structure of unit formula weight 339 were found in close agreement with analytically found percentages of elements. The calculated percentages of elements in their complexes with the monomer structure of unit formula weight 438 also accorded with the analytically found percentages of elements and estimated chlorine percentages. The calculated percentages in CSAPTSC and CCSAPTSC, corresponding to the monomer structure of unit formula weight 353 showed close correspondence with the analytically found percentages of elements. The calculated percentages corresponding to the monomer structure of unit formula weight 452 of their complexes were also in correspondence to the analytically found percentages of elements and estimated chlorine percentages. The analytically found percentages showed the substantial ranges of *DS* (Pires et al., 2013; Qin et al., 2012; Inukai et al., 1998; Melo et al., 2002) with 19.42–19.83 % *DS* in salicylaldehyde chitosan thiosemicarbazones and 31.68–31.74 % *DS* in acetyl phenol chitosan thiosemicarbazones. The percentages were indicatives of partial substitution of amino group in chitosan by thiosemicarbazone group and the analytically found percentages of elements in the complexes showed the coordination behavior of chitosan thiosemicarbazones. The calculated percentages of elements were based on the structures with completely deacetylated ring of chitosan. The *DS* values showed an agreement with decreased sulphur percentage with some variations in percentages of other elements in the derivatives formed by partial deacetylation of chitin, partial introduction of Schiff base group into chitosan (Qin et al., 2012), and more functionalization of commercial oligo chitosan than high molecular weight crab shell chitosan. The non-functionalized chitosan also forms the complex in a parallel reaction, and this is justified by higher percentage of estimated chlorine than calculated chlorine percentage.

3.1.5. Thermal studies

Thermogravimetric/differential thermal analysis (TG/DTA) curves of chitosan thiosemicarbazones (Figs. S21-S24 in supporting information) and the thermal data presented in Table 2 showed the thermal decomposition in two stages corresponding to weight loss due to the loss of water at 145–205 °*C* and weight loss due to the disruption of backbone linkage and thermal degradation of glucosamine residue at 200–1000 °*C*. In particular, there was a weight loss of 6.68 % at 150 °*C* in CSSTSC, 5.86 % at 205 °*C* in CCSSTSC, 5.29 % at 147 °*C* in CSAPTSC and 5.36 % at 145 °*C* in CCSAPTSC, and a weight loss of 79 % in CSSTSC, 74 % in CCSSTSC, 88 % in CSAPTSC, and 86 % in CCSAPTSC at 200–1000 °*C*. This behavior reasonably showed analogy with the reported temperature of loss of water in chitosan at 80–160 °*C* (Qin et al., 2012; Kittur et al., 2002) and decomposition temperatures of chitosan at 50–100 °*C* and 400 – 500 °*C* (Andrade et al., 2012; Kumari et al., 2017). The two stages of weight loss of commercial chitosan *viz.* 9 % of weight loss at 120 °*C* due to loss of water and 43 % of weight loss at 500 °*C* due to degradation of main chain of chitosan (Chethan et al., 2013; De Britto & Campana-Filho, 2004; Xu et al., 2010) have been reported, and in close agreement to this, there was 4.05–4.88 % weight loss due to loss of water at 120 °*C* and 65–69 % weight loss due to chain degradation at 500 °*C* in chitosan thiosemicarbazones. It showed more degradation of chitosan thiosemicarbazones than chitosan at the moderate heating in the range of 400 °*C* to 500 °*C*. There was a rapid rate of decomposition from 100 °*C* to 400 °*C* like in chitosan and then a steady rate of

Table 2
TG/DTA data of thermal events in chitosan thiosemicarbazones: salicylaldehyde and 2-acetylphenol analogues.

Compounds	Temperature (°*C*)	Weight loss (%)	Thermal event	% residue at 1000 °*C*
CSSTSC	150	6.68	Loss of water	
	200–1000	79	Chain disruption and backbone degradation	15
CCSSTSC	205	5.86	Loss of water	
	200–1000	74	Chain disruption and backbone degradation	14
CSAPTSC	147	5.29	Loss of water	
	200–1000	88	Chain disruption and backbone degradation	5
CCSAPTSC	145	5.36	Loss of water	
	200–1000	86	Chain disruption and backbone degradation	6

Table 1
The powder X ray diffraction data of chitosan thiosemicarbazones and their copper(II) complexes: salicylaldehyde and 2-acetylphenol analogues.

Compounds	Selected functionality peaks, 2θ Thiosemicarbazone crystallinity	Chitosan complex crystallinity	D (*nm*)	C.I (%)
CSSTSC	15.39°, 16.15°, 17.86°, 25.30°	–	16.57	72.84
Cu-CSSTSC	6.5°, 7.7°, 8.8°, 9.63°, 17.46°, 19.41°, 23.93°	12.57°,19.98°,25.07°	9.02	47.77
CCSSTSC	11.39°, 15.37°, 21.53°, 22.78°, 26.91°	-	15.53	71.97
Cu-CCSSTSC	9.60°, 12.45°, 13.02°,16.80°, 21.86°, 22.37°	13.92°,18.89°, 25.36°	10.20	45.12
CSAPTSC	8.40°,12.92°,22.28°,25.87°,28.47°, 29. 98°	-	24.76	42.96
Cu-CSAPTSC	18.01°, 22.01°, 23.13°, 23.60°	14.26°,19.98°, 24.14°	4.88	51.15
CCSAPTSC	9.2°, 12.8°, 19.04°, 22.48°, 25.38°, 26.54°, 29.40°	–	22.28	42.26
Cu-CCSAPTSC	7.70°, 11.26°, 15.60°, 17.78°	12.96°,19.82°,29.00°, 40.22°	6.39	49.47

decomposition, leaving about 14–15 % salicylaldehyde-based ligands and 5–6 % 2-acetyl phenol-based ligands as residue of the unsaturated structure at 1000 °*C*. Such a behavior was eventually attributed to reasonably high thermal stability of thiosemicarbazones (Qu et al., 2000). The two DTA peaks of chitosan thiosemicarbazones showed the correspondence to TG weight loss in two steps at the range of 25- 200 °*C* and 400–700 °*C*.

The TGA curves of complexes (Figs. S25-S28 in supporting information) and the thermal data presented in Table 3 showed the weight loss in three steps corresponding to the steady loss of weight up to 150-200 °*C*, rapid loss of weight at 200–500 °*C*, and again a steady loss of weight from 500 to 1000 °*C*. In particular, there was a weight loss of 12.66 % in Cu-CSSTSC, 1.08 % in Cu-CCSSTSC, 5.14 % in Cu-CSAPTSC and 1.06 % in Cu-CCSAPTSC at 200 °*C*, and a weight loss of about 42 % in Cu-CSSTSC, 78 % in Cu-CCSSTSC, 60 % in Cu-CSAPTSC, and 53 % in Cu-CCSAPTSC at 200–500 °*C*. It showed more degradation of complexes at the moderate heating in the lower range of temperature at 200–500 °*C* and then a steady rate of decomposition, leaving about 15–35 % as residue of the unsaturated structure at 700 °*C*. High molecular weight chitosan complexes were stable up to 200 °*C*. Such a behavior was attributed to reasonably standard thermal stability (Kittur et al., 2002; Qu et al., 2000) of complexes.

3.1.6. *Magnetic susceptibility measurement and electron paramagnetic resonance (EPR) spectroscopy*

Magnetic susceptibility measurement showed the effective magnetic moment (μ_{eff}) values of the complexes in the range of 1.80–1.85 *BM*, close to spin-only moment of 1.73 *BM* due to an unpaired electron. This indicated a low spin-spin coupling between unpaired electrons of different copper atoms (Ahmed & Lal, 2017) and some increase in the moment was attributed to large spin orbit coupling constant of cupric ion (Djord jevic, 1960). Magnetic moment of <1.90 *BM* indicated the square planar or octahedral stereochemistry of the complexes (Figgis, 1958).

The EPR spectra of complexes (Figs. S29–S32 in supporting information) were characterizable by axial g tensors (Bennur et al., 2001) and the non-resolution of hyperfine features due to copper ($S = 1/2$ and $I = 3/2$) was owing to intermolecular spin-spin interactions and dimeric association of molecules (Bhadbhade & Srinivas, 1993; Suresh et al., 1996). It meant that the absence of hyperfine splitting was attributed to exchange broadening due to still incomplete separation of paramagnetic centers at a low X-band frequency of 9.8 *GHz* (Farra et al., 2011). The EPR spectra corresponding to an unpaired electron in d $^{2}_{xy}$ orbital of Cu (II) centers were in further agreement with a square planar geometry (Garribba & Micera, 2006), but the g parallel tensors were undetectable due to absence of hyperfine splitting. The g values were 2.07 for Cu-CSSTSC (ν = 9.8623 *GHz*, B_o=3400 *Gs* = 340 *mT*), 2.10 for Cu-CCSSTSC (ν =9.8630 *GHz*, B_o = 3350 *Gs* = 335 *mT*), 2.09 for Cu-CSAPTSC (ν =9.8623 *GHz*, B_o = 3359 *Gs* = 335.9 *mT*), and 2.09 for Cu-CCSAPTSC (ν =9.8628 *GHz*, B_o = 3356 *Gs* = 335.6 *mT*). The shifting of g value from g_e (2.0023) that is due to spin orbital coupling of metal orbitals with unpaired electrons has been reported to depend upon the degree of covalency of the complex that is determined by the unpaired electron density at the donor atoms of ligand molecule (Ahmed & Lal, 2017). The absence of half field peak at 1500 Gauss suggesting the absence of two copper centers in the same lacuna indicated the mononuclear structure of the complexes (Patel & Sadasivan, 2017).

On the basis of the aforementioned results, the copper(II) complexes were proposed to assume the mononuclear distorted square planar geometry (Fig. 1). The thione sulphur, azomethine nitrogen, hydroxy group of salicylaldehyde or 2-acetylphenol moiety, and one chlorine atom were used as the donor sites in coordination with copper(II) ion in the complexes.

3.2. *Anticancer activity*

The *in vitro* antitumorigenic and anticancer activity profiles of chitosan oligosaccharide and high molecular weight crab shell chitosan as shown by the MTT cell viability assays against the MDCK, MCF-7 cell lines and the mouse normal embryonic fibroblast (NIH3T3) cells are presented in Table 4.

The *in vitro* antitumorigenic and anticancer activity profiles of chitosan oligosaccharide and high molecular weight crab shell chitosan functionalized thiosemicarbazones and their copper(II) complexes as shown by the MTT cell viability assays against the MDCK, MCF-7 cell lines and the mouse normal embryonic fibroblast (NIH3T3) cells are presented in Tables 5 & 6 respectively.

The anticancer activities of the compounds as revealed by colorimetric MTT assay were found as CS (IC_{50} (μgmL^{-1}): >400 in MDCK and 370 in MCF-7 cells); CCS(IC_{50} μgmL^{-1}): >400 in both MDCK and MCF-7 cells); chitosan oligosaccharide salicylaldehyde thiosemicarbazone *viz.*

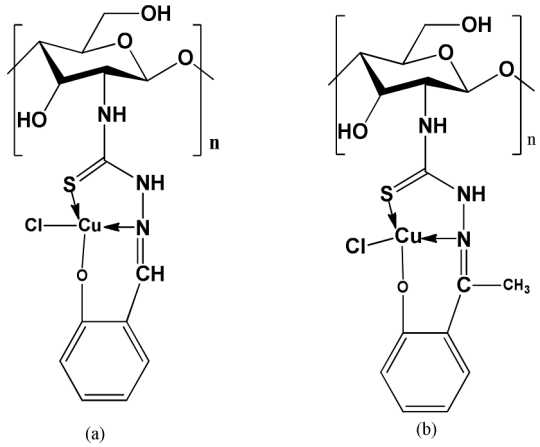

Fig. 1. Proposed structure of complexes: (a). Cu-CSSTSC and Cu-CCSSTSC (b). Cu-CSAPTSC and Cu-CCSAPTSC.

Table 3
TGA data of thermal events in copper(II) chitosan thiosemicarbazones: salicylaldehyde and 2-acetylphenol analogues.

Compounds	Temperature (°C)	Weight loss%	Thermal event	% residue at 700 °C
Cu-CSSTSC	200	12.66	Loss of water	35
	200–500	42	Disruption of the chain	
	500–700	10	Further degradation of the backbone	
Cu-CCSSTSC	200	1.08	Loss of water	15
	200–500	78	Disruption of the chain	
	500–700	06	Further degradation of the backbone	
Cu-CSAPTSC	200	5.14	Loss of water	30
	200–500	60	Disruption of the chain	
	500–700	05	Further degradation of the backbone	
Cu-CCSAPTSC	200	1.06	Loss of water	30
	200–500	53	Disruption of the chain	
	500–700	16	Further degradation of the backbone	

Table 4
The *in vitro* activity profile against MDCK, MCF-7 cell lines and NIH3T3 cells by chitosan oligosaccharide (CS) and high molecular weight crab shell chitosan (CCS).

Compounds	Activity against MDCK cell line Cell viability% (at 50–400 μgmL^{-1})	IC_{50} (μgmL^{-1}) ± *S.D.*	Activity against MCF-7cell line Cell viability% (at 50–400 μgmL^{-1})	IC_{50} (μgmL^{-1}) ± *S.D.*	Activity against NIH3T3 cells Cell viability% (at 50–600 μgmL^{-1})	IC_{50} (μgmL^{-1}) ± *S.D.*
CS	91–62	>400	91–44	370 ± 9.2	95–66	>600
CCS	96–78	>400	83–53	>400	98–84	>600

S.D. = Standard Deviation from the mean at $n = 3$.

Table 5
The *in vitro* activity profile against MDCK, MCF-7 cell lines and NIH3T3 cells proliferation by chitosan oligosaccharide thiosemicarbazones (CS TSC series) and their copper(II) complexes.

Compounds	Activity against MDCK cell line Cell viability% (at 50–400 μgmL^{-1})	IC50 (μgmL^{-1}) ± *S.D.*	Activity against MCF-7cell line Cell viability% (at 50–400 μgmL^{-1})	IC50 (μgmL^{-1}) ± *S.D.*	Activity against NIH3T3 cells Cell viability% (at 50–600 μgmL^{-1})	IC50 (μgmL^{-1}) ± *S.D.*
CSSTSC	80–28	334 ± 6.6	82–44	343 ± 8.2	96–72	>600
Cu-CSSTSC	83–25	258 ± 7.0	90–33	222 ± 7.5	95–71	>600
CSAPTSC	60–30	336 ± 8.2	79–39	341± 7.8	96–67	>600
Cu-CSAPTSC	91–30	312 ± 8.6	84–20	262 ± 8.0	96–64	>600

S.D. = Standard Deviation from the mean at $n = 3$.

Table 6
The *in vitro* activity profile against MDCK, MCF-7 cell lines and NIH3T3 cells proliferation by high molecular weight crab shell chitosan thiosemicarbazones (CCS TSC series) and their copper(II) complexes.

Compounds	Activity against MDCK cell line Cell viability% (at 50–400 μgmL^{-1})	IC50 (μgmL^{-1}) ± *S.D.*	Activity against MCF-7cell line Cell viability% (at 50–400 μgmL^{-1})	IC_{50} (μgmL^{-1}) ± *S.D.*	Activity against NIH3T3 cells Cell viability% (at 50–600 μgmL^{-1})	IC_{50} (μgmL^{-1}) ± *S.D.*
CCSSTSC	81–59	>400	78–49	393 ± 6.0	95–68	>600
Cu-CCSSTSC	84–46	391 ± 6.8	76–48	370 ± 6.6	92–64	>600
CCSAPTSC	75–33	356 ± 7.4	80–52	>400	96–66	>600
Cu-CCSAPTSC	80–34	334 ± 7.6	74–16	283 ± 6.2	93–63	>600

S.D. = Standard Deviation from the mean at $n = 3$.

CSSTSC (IC_{50} (μgmL^{-1}): 334 in MDCK and 343 in MCF-7 cells); copper (II) chitosan oligosaccharide salicylaldehyde thiosemicarbazone *viz.* Cu-CSSTSC (IC_{50} (μgmL^{-1}): 258 in MDCK and 222 in MCF-7 cells); crab shell chitosan salicylaldehyde thiosemicarbazone *viz.* CCSSTSC (IC_{50} (μgmL^{-1}): >400 in MDCK and 393 in MCF-7 cells); copper(II) crab shell chitosan salicylaldehyde thiosemicarbazone *viz.* Cu-CCSSTSC (μgmL^{-1}): 391 in MDCK and 390 in MCF-7 cells); chitosan oligosaccharide 2-acetylphenol thiosemicarbazone *viz.* CSAPTSC (IC_{50} (μgmL^{-1}): 336 in MDCK and 341 in MCF-7 cells); copper(II) chitosan oligosaccharide 2-acetylphenol thiosemicarbazone *viz.* Cu-CSAPTSC (IC_{50} (μgmL^{-1}): 312 in MDCK and 262 in MCF-7 cells); crab shell chitosan 2-acetylphenol thiosemicarbazone *viz.* CCSAPTSC (IC_{50} (μgmL^{-1}): 356 in MDCK and >400 in MCF-7 cells); and copper(II) crab shell chitosan 2-acetylphenol thiosemicarbazone *viz.* Cu-CCSAPTSC (IC_{50} (μgmL^{-1}): 354 in MDCK and 212 in MCF-7 cells). The hetero monomeric units of these compounds comprised the non-deacetylated chitin component, thiosemicarbazone moiety and unfunctionalized chitosan. The quantitative determination of unit monomer weight with all these structural contributions was further interfered by *DDA* and *DS* variations in reaction conditions, depolymerization and protonation effects, and copper(II)- chitosan complex formation in a parallel reaction. The IC_{50} values were hence expressed in $\mu g\ mL^{-1}$ rather than $\mu mol\ mL^{-1}$.

The results accorded with (i) anticancer enhancement upon the functionalization of chitosan as chitosan thiosemicarbazones, (ii) higher activity of oligo-chitosan thiosemicarbazones *viz.* CSTSC series than crab shell chitosan thiosemicarbazones *viz.* CCSTSC series, and (iii) an enhancement in anticancer activity with the increase in *DDA* and decrease in *Mw* of chitosan unit in the derivatives. Better enhancement in anticancer activity was observable in the copper(II) complex of 2-acetylphenol crab shell chitosan thiosemicarbazone than the corresponding complex of salicylaldehyde thiosemicarbazone, but this tendency was unfounded by the anticancer activity profiles of the corresponding complexes of chitosan oligosaccharide thiosemicarbazone. An enhancement in the *in vitro* activity upon the ONS tridentate coordination of phenolic carbaldehyde chitosan thiosemicarbazones with copper (II) ion may have been associated with the reportedly higher redox behavior of copper(II)-chitosan complexes than chitosan (West & Liberta, 1993). The lower viability of the MCF-7 cancer cells than the tumorigenic MDCK cells as shown by most of the assays may be attributed to preferential permeability of chitosan biomaterials through the more negatively charged cancer cell surfaces (Zhou et al., 2015).

Both the low molecular weight chitosan with high *DDA* and high molecular weight chitosan with low *DDA* have been reported to have low toxicity (IC_{50} > 4000 μgmL^{-1}) on normal cells (Chaudhry et al., 2021). It shows that the cytotoxicity of chitosan against the normal cells is minimal over a wide range of *Mw* and *DDA*. Doxorubicin as an anticancer drug in clinical use has been reported to show high cytotoxic effect (IC_{50} 0.68 μgmL^{-1}) in MCF-7 cells (Fang et al., 2014) and low toxicity (IC_{50} > 1350 μgmL^{-1}) in normal human dermal fibroblast (NHDF) cells (Tiago et al., 2014). Based on the conspicuous anticancer activity against MDCK and MCF-7 cells and lower toxicity to normal fibroblast NIH3T3 cells (IC_{50} >600 μgmL^{-1}), these chitosan functionalized thiosemicarbazones and their copper(II) complexes could stand as strategically favorable anticancer alternatives with minimal side effects. The results meanwhile accorded with the potential cytotoxicity of synthesized chitosan-functionalized thiosemicarbazones and their copper

(II) complexes in a dose and concentration dependent manner against the normal fibroblast NIH3T3 cells. The cellular metabolic activity of tumorigenic and cancer cells was measured by the colorimetric MTT assay. The tetrazolium dye MTT was reduced into its purple colored insoluble formazan by nicotinamide adenine dinucleotide phosphate (NADPH)-dependent cellular oxidoreductase enzyme and hence the cell viability percentages showed the correspondence with reductive activity of cellular dehydrogenases in mitochondria of living cells (Lu et al., 2012). The absorbance at 551 nm of the colored solution obtained by dissolution of purple formazan product by dimethyl sulfoxide (DMSO) was quantified to analyze the cell viability and proliferation. This process involving the cellular uptake of MTT by endocytosis, reduction of MTT by mitochondrial enzymes and the transfer of MTT to cell surfaces to form MTT-formazan crystals (Lu et al., 2012) corresponded to cellular metabolism and viability, and cytotoxicity of the samples. The reduction in cell viability as a measure of the metabolic events leading to cell death was shown by MTT assay as a technique of correlating the apoptotic progression (Henslee et al., 2016). Further, the mechanistic investigation of anticancer activity of these chitosan derivatives could be streamlined on the basis of the reported mechanisms of anticancer activity of salicylaldehyde-based TSCs associated with the interference to cancer cells proliferation caused by cellular protein folding (Carcelli et al., 2020; Yang et al., 2022), and the anticancer activity of copper(II) thiosemicarbazones associated with DNA disruption and apoptosis of cancer cells (Singh et al., 2020). The results also accorded with the enhancement in bioactivity upon the modification of native chitosan (Panda et al., 2019), increased pharmaceutical properties of chitosan functionalized Schiffs bases (Thakur & Bhalla, 2024), increased activity of salicylaldehyde-chitosan Schiffs base metal complexes against MCF-7 cancer cells (Barbosa et al., 2017), and in overall, the biocompatibility of chitosan derived materials in favor of biomedical applications (Panda et al., 2023; Panda et al., 2021).

4. Conclusion

Commercially available chitosan oligosaccharide and a high polymeric crab shell chitosan were partially grafted into thiosemicarbazone to get chitosan functionalized thiosemicarbazones. This process involved a one pot synthesis of chitosan thiosemicarbazide and the subsequent condensation of this intermediate with 2-acetylphenol or salicylaldehyde. Copper(II) chitosan thiosemicarbazones showed the ONS tridentate coordination from chitosan thiosemicarbazone and the next coordination was satisfied by a chloride ion to assume their square planar geometry in the coordination sphere. The synergizing anticancer effects of the constituent moieties were revealed by higher activity of chitosan thiosemicarbazone ligands than native chitosan. Anticancer activity was found further enhanced upon the coordination of chitosan thiosemicarbazones with copper(II) ion, irrespective of the *DDA* and M_w of constituent chitosan. Further, the *in vitro* inhibitory effects were found analogous in both the MCF-7 cancer cells and the tumorigenic MDCK cells. The current work of biomaterial chitosan tailoring comprising the syntheses of chitosan functionalized thiosemicarbazones and their copper(II) complexes associated with further investigation of mechanism of action of their anticancer activity could be crucial towards functional approaches of anticancer drug development strategy.

CRediT authorship contribution statement

Hari Sharan Adhikari: Methodology. **Aditya Garai:** Formal analysis. **Chetana Khanal:** Data curation. **Paras Nath Yadav:** Supervision.

Declaration of competing interest

No conflict of interest exists among the authors to declare.

Data availability

No data was used for the research described in the article.

Supporting information

Characterizing spectra, X ray diffractograms and thermo analytical curves of chitosan oligosaccharide and high molecular weight crab shell chitosan functionalized phenolic carbaldehyde thiosemicarbazones and their copper(II) complexes *viz.* FT-IR spectra: chitosan salicylaldehyde thiosemicarbazones, chitosan 2-acetylphenol thiosemicarbazones and the corresponding copper(II) chitosan thiosemicarbazone complexes, ^{13}C NMR spectra: chitosan salicylaldehyde thiosemicarbazones and chitosan 2-acetylphenol thiosemicarbazones, Powder X ray diffractograms: chitosan salicylaldehyde thiosemicarbazones, chitosan 2-acetylphenol thiosemicarbazones and the corresponding copper(II) chitosan thiosemicarbazone complexes, TG/DTA curves: chitosan salicylaldehyde thiosemicarbazones and chitosan 2-acetylphenol thiosemicarbazones, TG curves: copper(II) chitosan salicylaldehyde thiosemicarbazones and copper(II) chitosan 2-acetylphenol thiosemicarbazones, EPR spectra: copper(II) chitosan salicylaldehyde thiosemicarbazones and copper(II) chitosan 2-acetylphenol thiosemicarbazones.

Acknowledgments

We acknowledge Nepal Academy of Science and Technology (NAST), Indian National Science Academy (INSA) and Central Department of Biotechnology, Tribhuvan University, Kathmandu, Nepal. We are thankful to Professor A. R. Chakravarty, Department of Inorganic and Physical Chemistry, Indian Institute of Science, Bangalore, India. We thank Dr Agni Koirala, Sogang University, Department of Chemistry, Korea Center for Artificial Photosynthesis (KCAP), Centre for Nanomaterial, Shinsu-dong, Mapogo, South Korea. We acknowledge Shikhar Biotech, Lalitpur, Nepal for providing with the cell lines.

Supplementary materials

Supplementary material associated with this article can be found, in the online version, at doi:10.1016/j.carpta.2024.100469.

References

Abedian, Z., Moghadamnia, A. A., Zabihi, E., Pourbagher, R., Ghasemi, M., Nouri, H. R., et al. (2019). Anticancer properties of chitosan on osteosarcoma, breast cancer and cervical cancer cell lines. *Caspian Journal of Internal Medicine, 10*(4), 439–446.

Adhikari, H. S., & Yadav, P. N. (2018). Anticancer activity of chitosan, chitosan derivatives, and their mechanism of action. *International Journal of Biomaterials*, 1–29. Article ID 2952085.

Adhikari, H. S., Garai, A., Khanal, C., Adhikari, R., & Yadav, P. N. (2021a). Imidazole-2-carboxaldehyde chitosan thiosemicarbazones, and their copper(II) complexes: synthesis, characterization, and antitumorigenic activity against madin-darby canine kidney cell line. *Chemistry: Asian Journal of Chemistry, 33*, 969–976.

Adhikari, H. S., Garai, A., Marasini, B. P., Adhikari, R., & Yadav, P. N. (2021b). Synthesis and characterization of high molecular weight chitosan, and antioxidant activity of its chitosan oligosaccharide encapsulation. *Journal of Nepal Chemical Society, 42*(1), 29–38.

Adhikari, H. S., Garai, A., Thapa, M., Adhikari, R., & Yadav, P. N. (2022a). Chitosan functionalized thiophene-2-thiosemicarbazones, and their copper(II) complexes: Synthesis, characterization, and anticancer activity. *Journal of Macromolecular Science, 59*, 211–227.

Adhikari, H. S., Garai, A., Manandhar, K. D., & Yadav, P. N. (2022b). Pyridine-based NNS tridentate chitosan thiosemicarbazones and their copper(II) complexes: synthesis, characterization, and anticancer activity. *ACS Omega, 7*, 30978–30988.

Ahmed, A., & Lal, R. A. (2017). Synthesis, characterization and electrochemical studies of copper(II) complexes derived from succinoyl- and adipoyldihydrazones. *Arabian Journal of Chemistry, 10*, S901–S908.

Andrade, S., Ladchumananandasivam, R., Rocha, B., Belarmino, D., & Galvão, A. (2012). The use of exoskeletons of shrimp (Litopenaeus vanammei) and crab (Ucides cordatus) for the extraction of chitosan and production of nanomembrane. *Materials Sciences and Applications, 3*(7), 495–508.

Aneesrahman, K. N., Ramaiah, K., Rohini, G., Stefy, G. P., Bhuvanesh, N. S. P., & Sreekanth, A. (2019). Synthesis and characterisations of copper(II) complexes of 5-methoxyisatin thiosemicarbazones: Effect of N-terminal substitution on DNA/protein binding and biological activities. *Inorganica Chimica Acta, 492*, 131–141.

Anitha, A., Sowmya, S., Kumar, P. T. S., Deepthi, S., Chennazhi, K. P., Ehrlich, H., et al. (2014). Chitin and chitosan in selected biomedical applications. *Progress in Polymer Science, 39*, 1644–1667.

Antony, R., David, S. Theodore, Karuppasamy, K., Saravanan, K., Thanikaikarasan, S., & Balakumar, S. (2012). Structural, surface, thermal and catalytic properties of chitosan supported copper(II) mixed ligand complex materials. *Journal of surface engineered materials and advanced technology, 2*, 284–291.

Barbosa, H. F. G., Attjioui, M., Ferreira, A. P. G., Dockal, E. R., El Gueddari, N. E., Moerschbacher, B. M., et al. (2017). Synthesis, characterization and biological activities of biopolymeric schiff bases prepared with chitosan and salicylaldehydes and their Pd(II) and Pt(II) complexes. *Molecules, 22*(11) (Basel, Switzerland) (Basel, Switzerland)Article 1987.

Bennur, T. H., Srinivas, D., & Ratnasamy, P. (2001). EPR spectroscopy of copper and manganese complexes encapsulated in zeolites. *Microporous and Mesoporous Materials : the Official Journal of the International Zeolite Association, 48*, 111–118.

Bhadbhade, M. M., & Srinivas, D. (1993). Effects on molecular association, chelate conformation, and reactivity toward substitution in copper Cu(5-X-salen) complexes, salen2- = N, N'-ethylenebis(salicylidenaminato), X = H, CH_3O, and Cl: Synthesis, x-ray structures, and EPR investigations. *Inorganic Chemistry, 32*(24), 5458–5466.

Bharti, N., Shailendra, S. Sharma, Naqvi, F., & Azam, A. (2003). New palladium(II) complexes of 5-nitrothiophene-2-carboxaldehyde thiosemicarbazones: Synthesis, spectral studies and in vitro anti-amoebic activity. *Bioorganic & Medicinal Chemistry, 11*(13), 2923–2929.

Carcelli, M., Tegoni, M., Bartoli, J., Marzano, C., Pelosi, G., Salvalaio, M., et al. (2020). *In vitro* and *in vivo* anticancer activity of tridentate thiosemicarbazone copper complexes: Unravelling an unexplored pharmacological target. *European Journal of Medicinal Chemistry, 194*, 1–15. Article 112266.

Chaudhry, G. E., Thirukanthan, C. S., NurIslamiah, K. M., Sung, Y. Y., Sifzizul, T. S. M., & Effendy, A. W. M. (2021). Characterization and cytotoxicity of low-molecular-weight chitosan and chito-oligosaccharides derived from tilapia fish scales. *Journal of Advanced Pharmaceutical Technology & Research, 12*(4), 373–377.

Chethan, P. D., Vishalakshi, B., Sathish, L., Ananda, K., & Poojary, B. (2013). Preparation of substituted quaternized aryl furan chitosan derivatives and their antimicrobial activity. *International Journal of Biological Macromolecules, 59*, 158–164.

Comsa, Ş., Cimpean, A. M., & Raica, M. (2015). The story of MCF-7 breast cancer cell line: 40 years of experience in research. *Anticancer Research, 35*(6), 3147–3154.

Cruz-Romero, M. C., Murphy, T., Morris, M., Cummins, E., & Kerry, J. P. (2013). Antimicrobial activity of chitosan, organic acids and nano-sized solubilisates for potential use in smart antimicrobially-active packaging for potential food applications. *Food Control, 34*, 393–397.

De Angelis, A. A., Capitani, D., & Crescenzi, V. (1998). Synthesis and ^{13}C CP-MAS NMR characterization of a new chitosan-based polymeric network. *Macromolecules, 31*, 1595–1601.

De Britto, D., & Campana-Filho, S. P. (2004). A kinetic study on the thermal degradation of N, N, N-trimethylchitosan. *Polymer Degradation and Stability, 84*(2), 353–361.

Dehaghi, S. M., Rahmanifar, B., Moradi, A. M., & Azar, P. A. (2014). Removal of permethrin pesticide from water by chitosan–zinc oxide nanoparticles composite as an adsorbent. *Journal of Saudi Chemical Society, 18*, 348–355.

de Britto, D., & Assis, O. B. G. (2007). A novel method for obtaining a quaternary salt of chitosan. *Carbohydrate Polymers, 69*, 305–310.

Denoyer, D., Masaldan, S., Fontaine, S. La, & Cater, M. A. (2015). Targeting copper in cancer therapy: "copper that cancer. *Metallomics : Integrated Biometal Science, 7*(11), 1459–1476.

Djord jevic, C. (1960). Magnetic susceptibilities of some square four-covalent and tetragonal six-covalent complexes of divalent copper. *Croatica Chemica Acta Arhiv za Kemiju, 32*(4), 183–187.

Fang, X. J., Jiang, H., Zhu, Y. Q., Zhang, L. Y., Fan, Q. H., & Tian, Y. (2014). Doxorubicin induces drug resistance and expression of the novel CD44st via NF-κB in human breast cancer MCF-7 cells. *Oncology Reports, 31*(6), 2735–2742.

Faris, T., Harisa, G. I., Alanazi, F. K., Badran, M. M., Alotaibi, A. M., Almanea, H., et al. (2021). Cytotoxicity of chitosan ultrafine nanoshuttles on the MCF-7 cell line as a surrogate model for breast cancer. *Current Drug Delivery, 18*(1), 19–30.

Farra, R., Thiel, K., Winter, A., Klamroth, T., Pöppl, A., Kelling, A., et al. (2011). Tetrahalidocuprates(II)—Structure and EPR spectroscopy. Part 1: Tetrabromidocuprates(II). *New Journal of Chemistry, 35*, 2793–2803.

Figgis, B. N. (1958). Magnetic properties of spin-free transition series complexes. *Nature, 182*, 1568–1570.

Finch, R. A., Liu, M. C., Grill, S. P., Rose, W. C., Loomis, R., Vasquez, K. M., et al. (2000). Triapine (3-aminopyridine-2-carboxaldehyde- thiosemicarbazone): A potent inhibitor of ribonucleotide reductase activity with broad spectrum antitumor activity. *Biochemical Pharmacology, 59*, 983–991.

Garribba, E., & Micera, G. (2006). The determination of the geometry of Cu(II) complexes: An EPR spectroscopy experiment. *Journal of Chemical Education, 83*(8), 1229–1232.

Geraki, K., Farquharson, M. J., & Bradley, D. A. (2002). Concentrations of Fe, Cu and Zn in breast tissue: A synchrotron XRF study. *Physics in Medicine and Biology, 47*(13), 2327–2339.

Gojo, I., Tidwell, M. L., Greer, J., Takebe, N., Seiter, K., Pochron, M. F., et al. (2007). Phase I and pharmacokinetic study of triapine, a potent ribonucleotide reductase inhibitor, in adults with advanced hematologic malignancies. *Leukemia Research, 31*, 1165–1173.

Hafdani, F. N., & Sadeghinia, N. (2011). A review on application of chitosan as a natural antimicrobial. *World Academy of Science, Engineering and Technology, 50*(2), 46–50.

Hanumantharao, R., Kalainathan, S., & Bhagavannarayana, G. (2012). Growth, spectral, optical, thermal, crystallization perfection and nonlinear optical studies of novel nonlinear optical crystal—urea thiosemicarbazone monohydrate. *Spectrochimica Acta Part A, Molecular and Biomolecular Spectroscopy, 91*, 345–351.

Henslee, E. A., Torcal Serrano, R. M., Labeed, F. H., Jabr, R. I., Fry, C. H., Hughes, M. P., et al. (2016). Accurate quantification of apoptosis progression and toxicity using a dielectrophoretic approach. *The Analyst, 141*(23), 6408–6415.

Hernández, W., Vaisberg, A. J., Tobar, M., Álvarez, M., Manzur, J., Echevarría, Y., et al. (2016). In vitro antiproliferative activity of palladium(II) thiosemicarbazone complexes and the corresponding functionalized chitosan coated magnetite nanoparticles. *New Journal of Chemistry, 40*, 1853–1860.

Huang, M., Khor, E., & Lim, L. Y. (2004). Uptake and cytotoxicity of chitosan molecules and nanoparticles: Effects of molecular weight and degree of deacetylation. *Pharmaceutical Research, 21*(2), 344–353.

Inukai, Y., Chinen, T., Matsuda, T., Kaida, Y., & Yasuda, S. (1998). Selective separation of germanium(IV) by 2,3- dihydroxypropyl chitosan resin. *Analytica Chimica Acta, 371*, 187–193.

Ismail, E. H., Sabry, D. Y., Mahdy, H., & Khalil, M. M. H. (2014). Synthesis and characterization of some ternary metal complexes of curcumin with 1,10-phenanthroline and their anticancer applications. *Journal of Scientific Research, 6*(3), 509–519.

Jiao, T. F., Zhou, J., Zhou, J. X., Gao, H., Xing, Y. Y., & Li, X. H. (2011). Synthesis and characterization of chitosan-based Schiff base compounds with aromatic substituent groups. *Iranian Polymer Journal, 20*(2), 123–136.

Jordan, M. A., & Wilson, L. (2004). Microtubules as a target for anticancer drugs. *Nature Reviews Cancer, 4*(4), 253–265.

Joseph, M., Kuriakose, M., Kurup, M. R. P., Suresh, E., Kishore, A., & Bhat, S. G. (2006). Structural, antimicrobial and spectral studies of copper(II) complexes of 2-benzoylpyridine N(4)-phenyl thiosemicarbazone. *Polyhedron, 25*(1), 61–70.

Kittur, F. S., Prashanth, K. V. H., Sankar, K. U., & Tharanathan, R. N. (2002). Characterization of chitin, chitosan and their carboxymethyl derivatives by differential scanning calorimetry. *Carbohydrate Polymers, 49*, 185–193.

Kucukgulmez, A., Celik, M., Yanar, Y., Sen, D., Polat, H., & Kadak, A. E. (2011). Physicochemical characterization of chitosan extracted from metapenaeous stebbingi shells. *Food Chemistry, 126*, 1144–1148.

Kumar, P., Nagarajan, A., & Uchil, P. D. (2018). Analysis of cell viability by the MTT assay. *Cold Spring Harbor Protocols*, (6), 469–471, 2018.

Kumari, S., Rath, P., & Sri Hari Kumar, A. (2016). Chitosan from shrimp shell (Crangon crangon) and fish scales (Labeo rohita): Extraction and characterization. *African Journal of Biotechnology, 15*(24), 1258–1268.

Kumari, S., Annamareddy, S. H. K., Abanti, S., & Rath, P. K. (2017). Physicochemical properties and characterization of chitosan synthesized from fish scales, crab and shrimp shells. *International Journal of Biological Macromolecules, 104*, 1697–1705.

Kumirska, J., Czerwicka, M., Kaczynski, Z., Bychowska, A., Brzozowski, K., Thöming, J., et al. (2010). Application of spectroscopic methods for structural analysis of chitin and chitosan. *Marine Drugs, 8*, 1567–1636.

Lomadze, N., & Schneider, H. J. A. (2005). Chitosan-based chemo mechanical polymer triggered by stacking effects with aromatic effectors including amino acid derivatives. *Tetrahedron, 61*, 8694–8698.

Lu, L., Zhang, L., Wai, M. S., Yew, D. T., & Xu, J. (2012). Exocytosis of MTT formazan could exacerbate cell injury. *Toxicology In Vitro, 26*(4), 636–644.

Malarz, K., Mrozek-Wilczkiewicz, A., Serda, M., Rejmund, M., Polanski, J., & Musiol, R. (2018). The role of oxidative stress in activity of anticancer thiosemicarbazones. *Oncotarget, 9*, 17689–17710.

Mekahlia, S., & Bouzid, B. (2009). Chitosan-Copper (II) complex as antibacterial agent: Synthesis, characterization and coordinating bond- activity correlation study. *Physics Procedia, 2*, 1045–1053.

Melo, M. R. S., Feitosa, J. P. A., Freitas, A. L. P., & de Paula, R. C. M. (2002). Isolation and characterization of soluble sulfated polysaccharide from the red seaweed Gracilaria cornea. *Carbohydrate Polymers, 49*(4), 491–498.

Muzzarelli, R. A. A., Tanfani, F., Mariotti, S., & Emanuelli, M. (1982). Preparation and characteristic properties of dithiocarbamate chitosan, a chelating polymer. *Carbohydrate Research, 104*, 235–243.

Nithya, A., & Jothivenkatachalam, K. (2015). Chitosan assisted synthesis of ZnO nanoparticles: An efficient solar light driven photocatalyst and evaluation of antibacterial activity. *Journal of Materials Science: Materials in Electronics, 26*(12), 10207–10216.

Omeir, R. L., Teferedegne, B., Foseh, G. S., Beren, J. J., Snoy, P. J., Brinster, L. R., et al. (2011). Heterogeneity of the tumorigenic phenotype expressed by Madin–Darby canine kidney cells. *Comparative Medicine, 61*(3), 243–250.

Panda, P. K., Yang, J. M., Chang, Y. H., & Su, W. W. (2019). Modification of different molecular weights of chitosan by p-Coumaric acid: Preparation, characterization and effect of molecular weight on its water solubility and antioxidant property. *International Journal of Biological Macromolecules, 136*, 661–667.

Panda, P. K., Yang, J. M., & Chang, Y. H. (2021). Preparation and characterization of ferulic acid-modified water soluble chitosan and poly (γ-glutamic acid) polyelectrolyte films through layer-by-layer assembly towards protein adsorption. *International Journal of Biological Macromolecules, 171*, 457–464.

Panda, P. K., Sadeghi, K., Park, K., & Seo, J. (2023). Regeneration approach to enhance the antimicrobial and antioxidant activities of chitosan for biomedical applications. *Polymers, 15*(1), 132. Article.

Patel, A., & Sadasivan, R. (2017). Microwave assisted one pot synthesis and characterization of Cesium salt of di-copper substituted phosphotungstate and its

application in the selective epoxidation of cis-cyclooctene with tert-butyl hydroperoxide. *Inorganica Chimica Acta, 458*, 101–108.
Pillai, C., Paul, W., & Sharma, C. P. (2009). Chitin and chitosan polymers: Chemistry, solubility and fiber formation. *Progress in Polymer Science, 34*(7), 641–678.
Pires, N. R., Cunha, P. L. R., Maciel, J. S., Angelim, A. L., Melo, V. M. M., de Paula, R. C. M., et al. (2013). Sulfated chitosan as tear substitute with no antimicrobial activity. *Carbohydrate Polymers, 91*, 92–99.
Polychronopoulos, P., Magiatis, P., Skaltsounis, A. L., Myrianthopoulos, V., Mikros, E., Tarricone, A., et al. (2004). Structural basis for the synthesis of indirubins as potent and selective inhibitors of glycogen synthase kinase-3 and cyclin-dependent kinases. *Journal of Medicinal Chemistry, 47*, 935–946.
Qin, Y., Xing, R., Liu, S., Li, K., Meng, X., Li, R., et al. (2012). Novel thiosemicarbazone chitosan derivatives: Preparation, characterization, and antifungal activity. *Carbohydrate Polymers, 87*, 2664–2670.
Qu, X., Wirsen, A., & Albertsson, A. (2000). Effect of lactic/glycolic acid side chains on the thermal degradation kinetics of chitosan derivatives. *Polymer, 41*, 4841–4847.
Ramya, R., Sudha, P. N., & Mahalakshmi, J. (2012). Preparation and characterization of chitosan binary blend. *International Journal of Scientific and Research Publications, 2*, 1–9.
Rao, V. A., Klein, S. R., Agama, K. K., Toyoda, E., Adachi, N., Pommier, Y., et al. (2009). The iron chelator Dp44mT causes DNA damage and selective inhibition of topoisomerase II alpha in breast cancer cells. *Cancer Research, 69*, 948–957.
Santhakumari, R., Ramamurthi, K., Vasuki, G., Yamin, B. M., & Bhagavannarayana, G. (2010). Synthesis and spectral characterization of acetophenone thiosemicarbazone—A nonlinear optical material. *Spectrochimica Acta Part A, Molecular and Biomolecular Spectroscopy, 76*, 369–375.
Santini, C., Pellei, M., Gandin, V., Porchia, M., Tisato, F., & Marzano, C. (2014). Advances in copper complexes as anticancer agents. *Chemical Reviews, 114*, 815–862.
Sarker, D., Karim, M. R., Haque, M. M., Zamir, R., & Asraf, M. A. (2019). Copper (II) complex of salicylaldehyde semicarbazone: Synthesis, characterization and antibacterial activity. *Asian Journal of Chemical Sciences, 6*(4), 1–8.
Sibuh, B. Z., Taneja, P., & Khanna, S. (2020). Effects of substituents on anticancer activity of thiosemicarbazone against MCF-7 human breast cancer cell line. *bioRxiv : The Preprint Server for Biology, 02*(19), Article 955690.
Singh, N. K., Kumbhar, A. A., Pokharel, Y. R., & Yadav, P. N. (2020). Anticancer potency of copper(II) complexes of thiosemicarbazones. *Journal of Inorganic Biochemistry, 210* (111134), 1–31.
Sobiesiak, M., Cieślak, M., Krolewsk, K., Kaźmierczak-Barańsk, J., Pasternak, B., & Budzisz, E. (2016). Thiosemicarbazone-derived copper(II), cobalt(II) and nickel(II) complexes as potential anticancer agents: Nuclease activity, cytotoxicity and apoptosis studies. *New Journal of Chemistry, 40*(11), 9761–9767.
Sun, L., Liang, C., Shirazian, S., Zhou, Y., Miller, T., Cui, J., et al. (2003). Discovery of 5-[5-fluoro-2-oxo-1,2-dihydroindol-(3Z)-ylidenemethyl]-2,4-dimethyl-1H-pyrrole-3-carboxylic acid (2-diethylaminoethyl) amide, a novel tyrosine kinase inhibitor targeting vascular endothelial and platelet-derived growth factor receptor tyrosine kinase. *Journal of Medicinal Chemistry, 46*, 1116–1119.
Suresh, E., Bhadbhade, M. M., & Srinivas, D. (1996). Molecular association, chelate conformation and reactivity correlations in substituted o-phenylenebis (salicylidenato) copper(II) complexes: UV-visible, EPR and X-ray structural investigations. *Polyhedron, 15*(23), 4133–4144.
Thakur, S., & Bhalla, A. (2024). Sustainable synthetic endeavors of pharmaceutically active Schiff bases and their metal complexes: A review on recent reports. *Tetrahedron, 153*, Article 133836. Article.
Tiago, M., de Oliveira, E. M., Brohem, C. A., Pennacchi, P. C., Paes, R. D., Haga, R. B., et al. (2014). Maria-Engler, Fibroblasts protect melanoma cells from the cytotoxic effects of doxorubicin. *Tissue Engineering Part A, 20*(17–18), 2412–2421.
Tiwari, D., Basnet, K., Lamichhane, J., Niraula, P., Bhandari, S., & Yadav, P. N. (2016). Copper complexes of imidazole-2-carbaldehyde N(4)-substituted thiosemicarbazones: synthesis, characterization and antimicrobial activity. *Chemistry: An Asian Journal, 28*(12), 2793–2797.
Tokarek, K., Hueso, J. L., Kustrowski, P., Stochel, G., & Kyziol, A. (2013). Green synthesis of chitosan-stabilized copper nanoparticles. *European Journal of Inorganic Chemistry, 28*, 4940–4947.
Usman, M. S., Ibrahim, N. A., Shameli, K., Zainuddin, N., & Yunus, W. M. Z. W. (2012). Copper nanoparticles mediated by chitosan: synthesis and characterization via chemical methods. *Molecules, 17*(12), 14928–14936 (Basel, Switzerland).
Vindya, N. G., Sharma, N., Yadav, M., & Ethiraj, K. R. (2015). Tubulins — the target for anticancer therapy. *Current Topics in Medicinal Chemistry, 15*, 73–82.
Wang, X., Du, Y., Fan, L., Liu, H., & Hu, Y. (2005). Chitosan- metal complexes as antimicrobial agent: Synthesis, characterization and Structure-activity study. *Polymer Bulletin, 55*, 105–113.
Wang, F., Jiao, P., Qi, M., Frezza, M., Dou, Q. P., & Yan, B. (2010). Turning tumor-promoting copper into an anti-cancer weapon via high-throughput chemistry. *Current Medicinal Chemistry, 17*(25), 2685–2698.
Wang, J., Jiang, J. Z., Chen, W., & Bai, Z. W. (2016). Data of $^{1}H/^{13}C$ NMR spectra and degree of substitution for chitosan alkyl urea. *Data in Brief, 7*, 1228–1236.
West, D. X., & Liberta, A. E. (1993). Thiosemicarbazone complexes of copper(II): Structural and biological studies. *Coordination Chemistry Reviews, 123*(1–2), 49–71.
Wiles, D. M., Gingras, B. A., & Suprunchuk, T. (1967). The C=S stretching vibration in the infrared spectra of some thiosemicarbazones. *Canadian Journal of Chemistry, 45*, 470–473.
Wimardhani, Y. S., Suniarti, D. F., Freisleben, H. J., Wanandi, S. I., Siregar, N. C., & Ikeda, M. A. (2014). Chitosan exerts anticancer activity through induction of apoptosis and cell cycle arrest in oral cancer cells. *Journal of Oral Science, 56*(2), 119–126.
Wu, S. J., Liou, T. H., & Mi, F. L. (2009). Synthesis of zero-valent copper-chitosan nanocomposites and their application for treatment of hexavalent chromium. *Bioresource Technology, 100*, 4348–4353.
Xie, H., & Kang, Y. J. (2009). Role of copper in angiogenesis and its medicinal implications. *Current Medicinal Chemistry, 16*, 1304–1314.
Xu, T., Xin, M., Li, M., Huang, H., & Zhou, S. (2010). Synthesis, characteristic and antibacterial activity of N, N, N-trimethyl chitosan and its carboxymethyl derivatives. *Carbohydrate Polymers, 81*, 931–936.
Yadav, H. K. S., & Shivakumar, H. G. (2012). In vitro and in vivo evaluation of pH-sensitive hydrogels of carboxymethyl chitosan for intestinal delivery of theophylline. *International Scholarly Research Notices*, 1–9. Article ID 763127.
Yamaguchi, A., Penland, R. B., Mizushima, S., Lane, T. J., Curran, C., & Quagliano, J. V. (1958). Infrared absorption spectra of inorganic coordination complexes. XIV. Infrared studies of some metal thiourea complexes. *Journal of the American Chemical Society, 80*, 527.
Yang, S., Jackson, C., Karapetyan, E., Dutta, P., Kermah, D., Wu, Y., et al. (2022). Roles of protein disulfide isomerase in breast cancer. *Cancers, 14*(3), 745.
Yoshida, D., Ikeda, Y., & Nakazawa, S. (1993). Quantitative analysis of copper, zinc and copper/zinc ratio in selected human brain tumors. *Journal of Neuro-Oncology, 16*, 109–115.
Zhang, Y. Q., Xue, C. H., Xue, Y., Gao, R. C., & Zhang, X. L. (2005). Determination of the degree of deacetylation of chitin and chitosan by X-ray powder diffraction. *Carbohydrate Research, 340*, 1914–1917.
Zhang, J., Xia, W., Liu, P., Cheng, Q., Tahirou, T., Gu, W., et al. (2010a). Chitosan modification and pharmaceutical/biomedical applications. *Marine Drugs, 8*(7), 1962–1987.
Zhang, J., Xia, W., Liu, P., Cheng, Q., Tahirou, T., Gu, W., et al. (2010b). Chitosan modification and pharmaceutical/biomedical applications. *Marine Drugs, 8*(7), 1962–1987.
Zhang, Z., Gou, Y., Wang, J., Yang, K., Qi, J., Zhou, Z., et al. (2016). Four copper(II) compounds synthesized by anion regulation: Structure, anticancer function and anticancer mechanism. *European Journal of Medicinal Chemistry, 121*, 399–409.
Zheng, Y., Yi, Y., Qi, Y., Wang, Y., Zhang, W., & Du, M. (2006). Preparation of chitosan-copper complexes and their antitumor activity. *Bioorganic & Medicinal Chemistry Letters, 16*(15), 4127–4129.
Zhong, Z., Zhong, Z., Xing, R., Li, P., & Mo, G. (2010). The preparation and antioxidant activity of 2-[phenylhydrazine (or hydrazine)-thiosemicarbazone]-chitosan. *International Journal of Biological Macromolecules, 47*(2), 93–97.
Zhong, Z., Aotegen, B., & Xu, H. (2011). The influence of the different inductivity of acetyl phenyl–thiosemicarbazone–chitosan on antimicrobial activities. *International Journal of Biological Macromolecules, 48*(5), 713–719.
Zhou, Y., Wong, C. O., Cho, K-j., van der Hoeven, D., Liang, H., Thakur, D. P., et al. (2015). Signal transduction. Membrane potential modulates plasma membrane phospholipid dynamics and K-Ras signaling. *Science, 349*(6250), 873–876 (New York, N.Y.).